Hindawi
International Journal of Antennas and Propagation
Volume 2019, Article ID 7691912, 7 pages
https://doi.org/10.1155/2019/7691912

Research Article

Millimetre-Wave Planar Phased Patch Array with Sidelobe Suppression for High Data-Rate Transmission

Hung-Chen Chen,[1] **Tsenchieh Chiu**,[1] **and Ching-Luh Hsu**[2]

[1]*National Central University, Taoyuan, Taiwan*
[2]*National Chung-Shan Institute of Science and Technology, Taoyuan, Taiwan*

Correspondence should be addressed to Tsenchieh Chiu; tcchiu@ee.ncu.edu.tw

Received 19 September 2019; Revised 21 November 2019; Accepted 5 December 2019; Published 20 December 2019

Academic Editor: Gino Sorbello

A design of 38 GHz planar phased patch array with sidelobe suppression for data-rate enhancement is proposed in the paper. The proposed array is formed of three 24-element subarrays of patches. Each patch has its own transmit/receive modules (TRM) consisting of a digitally controlled attenuator and phase shifter. In order to achieve high data-rate communications, the noise, especially due to the undesired signals received from the sidelobes, should be reduced with high sidelobe suppression of subarray. The sidelobe suppression of the proposed subarray is first improved to 17.92 dB with a diamond-shaped aperture and then better than 35 dB with a tapered radiation power distribution. The excellent sidelobe suppression of the antenna array is essential for the beam-division multiplexing applications when the signal sources are close to each other. The proposed design is validated experimentally, including the data-rate measurements showing that the 7 Gbps data transmission can be achieved with sufficient sidelobe suppression of the proposed design.

1. Introduction

Base-station antennas generally require beam steering or multibeam capability. Active electronically scanned array (AESA) is one of the promising antenna systems for the base stations, especially in the applications of the 5G technologies [1]. With AESA, the antenna beam can scan very fast and change direction in several microseconds. In [2], a switchable phased array composed of three 8-element subarrays of patch antennas is presented for the 5G systems. By controlling phase shifter assemblies, the subarray can cover a wide scanning range. When these arrays are used in multiple access communication systems, interference problems could be significant due to the poor sidelobe suppression. Signals received from sidelobes could lead to serious signal-to-noise ratio (SNR) degradation. Since the achieved data rate can grow as SNR is increased [3], the sidelobe suppression of the array should be enhanced to lessen the interference from the sidelobes and obtain desired data-rate performance.

Several techniques that aim at improving the sidelobe suppression have been shown in the literature. The technique of amplitude-only control is a simple method as it changes only the current amplitude excited at each element [4, 5]. In [6], the sidelobe level is kept at the desired value by using Taylor excited antennas. It is found that some radiated power is wasted in the quantization attenuators, resulting in poor power efficiency. The technique of position-only control with density taper can suppress sidelobes and keep high power efficiency [7]. Nevertheless, the degree of sidelobe suppression mainly depends on the number of array elements. In [8], the method of spectral factorization is applied to both uniformly and nonuniformly spaced linear arrays in which the mutual coupling and mounting-platform effects are present. The overall design procedure does not rely on any restriction on the nature and the shape of the fields. It is considered as a couple of convex optimizations plus a polynomial factorization. In [9], a technique is presented to place low sidelobes and nulls in desired directions by dynamically altering the thinning configuration of a

linear array. In [10], the adaptive beamforming algorithm with sidelobe suppression by introducing extra nulls into the radiation pattern is proposed. In [11], a density tapering algorithm is presented for the pencil beam synthesis of linear sparse arrays. In [12], the binomial distribution is achieved by using tapered patch width. The binomial array provides sidelobe suppression of 28 dB with 12.5 dBi gain at 5.76 GHz. Though there are many techniques available, the effect of the high sidelobe suppression on the data-rate performance should also be demonstrated.

In the paper, a design of millimetre-wave phased array with sidelobe suppression for data-rate enhancement will be presented. The proposed array is formed of three 24-element subarrays of patches and is operated at 38 GHz with 2 GHz bandwidth. Every patch has its own transmit/receive modules consisting of digitally controlled attenuator and phase shifter. The scan range of the subarray is of ±20 degrees. Due to the narrow scan range, the magnitude of the sidelobes close to the main beam of the subarrays should be significantly decreased to alleviate the interference from signal sources close to each other. The sidelobe suppression of the proposed array is first improved by deploying the elements of subarray in the diamond shape and then by adjusting the output power of each element. It is found that the sidelobe suppression in the scan range should be better than 35 dB to achieve the data rate better than 7 Gbps. In what follows, array configuration will be explained, the experiment results will be presented, and the conclusions will be given.

2. Antenna Array Design and Simulation

The proposed array formed of three subarrays is shown in Figure 1. With these subarrays, the system is capable of controlling three beams simultaneously for covering multidirections in the horizontal plane (*xz*-plane). The patch antennas in the array are realized on the Duroid 5880 substrate with $\varepsilon_r = 2.2$ and 10 mil in thickness. The dimension of the patch is $2.4 \times 2.17\ \text{mm}^2$. The subarray is deployed with the triangular grid, and the element spacing d*x* and d*y* is 5.2 mm and 3.0 mm, respectively. Due to the limited quantity of the TR modules, the element number of a subarray is chosen as 24.

In order to achieve the sidelobe suppression better than 35 dB in the scan range, two sidelobe-suppression techniques are used in the design: the density tapering as the elements of subarray are deployed in diamond-shaped aperture, and the adaptive nulling algorithm [10] for adjusting the radiation power of each elements. Generally, the rectangular aperture with the triangular grid, as shown in Figure 2, is often used. In the paper, in order to apply the density tapering technique, the subarray elements are deployed in a diamond-shaped aperture, as shown in Figure 3. The element numbers along the *x*-axis are 1, 1, 1, 2, 2, 3, 4, 3, 2, 2, 1, 1, and 1. The comparison between the rectangular and diamond-shaped apertures is given in Table 1. The element numbers in both apertures are the same (24 elements). While the peak gain almost remains the same (19.4 dBi), the sidelobe suppression is improved from 13.0 dB for rectangular aperture to 17.9 dB for the diamond-shaped aperture. Moreover, the 3 dB beamwidth in the *xz*-plane is decreased from 9.6 to 7.6 degrees.

In order to further improve the sidelobe suppression, the weighting power of each elements is adjusted by using adaptive nulling algorithm. The algorithm has iterative structures. In each iteration, the algorithm first finds the direction of the peak sidelobe and then finds proper element weighting that produces an extra null toward this direction. The flowchart of iterative procedure is given in Figure 4.

The calculated weighting power of each subarray elements is given in Figure 3, and the result of the sidelobe suppression is again given in Table 1. The sidelobe suppression is improved to 35.8 dB, while the peak gain of the subarray is decreased to 15.5 dBi. Figure 5 shows the comparison of simulated *xz*-plane normalized patterns of the three subarrays listed in Table 1. It can be seen that the sidelobes in the scan range are suppressed as expected.

Figures 6(a) and 6(b) show the photographs of the feeding networks and the fabricated array. In the network, a WR28 waveguide 4-way power combiner is first connected with three WR28 waveguide 8-way power combiners and a 50 ohms load. Each 8-way power combiner is then connected with eight Ka-band TRMs. The Ka-band TRM, as illustrated in Figure 6(c), integrates millimetre-wave components such as T/R switch [13] power amplifiers, power controllers, low-noise amplifiers, attenuators, and phase shifters. The P1dB of the transmitter and receiver gain are 27.1 dBm and 23.4 dB, respectively. The effective isotropic radiated power (EIRP) is better than 46 dBm. The noise figure of the LNA is less than 6.8 dB. The main beam of subarray can be pointed to the desired direction in the specified range by controlling the phase shifters. The 5-bit TGP2102 phase shifter [14] is employed to provide the required phase with 11.25° resolution. In addition to the density tapering effect due to the diamond-shaped aperture, the sidelobe suppression of subarray can be further improved by controlling the attenuators. The 5-bit HMC939 attenuator [15] is employed to adjust the power magnitude with 1 dB resolution. For the receiving pattern with sufficient sidelobe suppression in the *xz*-plane, the distributions of the amplitude and phase of the subarray elements can be selected from the precalculated look-up table. Digital compensation algorithms are also applied to increase the phase accuracy within ±5.625° and the amplitude accuracy within ±0.5 dB. For better understanding of the system design, the overall design procedure is given in Figure 7.

3. Experiment Results

Figure 8 shows the simulated [16] and measured reflection coefficients of the patch in the middle of the subarray (the patch is circled in the figure). Since the other patches are present during the simulation and measurement, it is found there are ripples along the traces due to the mutual coupling. The measured bandwidth is from 36 to 39.5 GHz with reflection coefficients below −10 dB. The radiation patterns and peak gains of the proposed subarray are measured by using the NSI-MI Vertical Planar Near-field system [17]. In

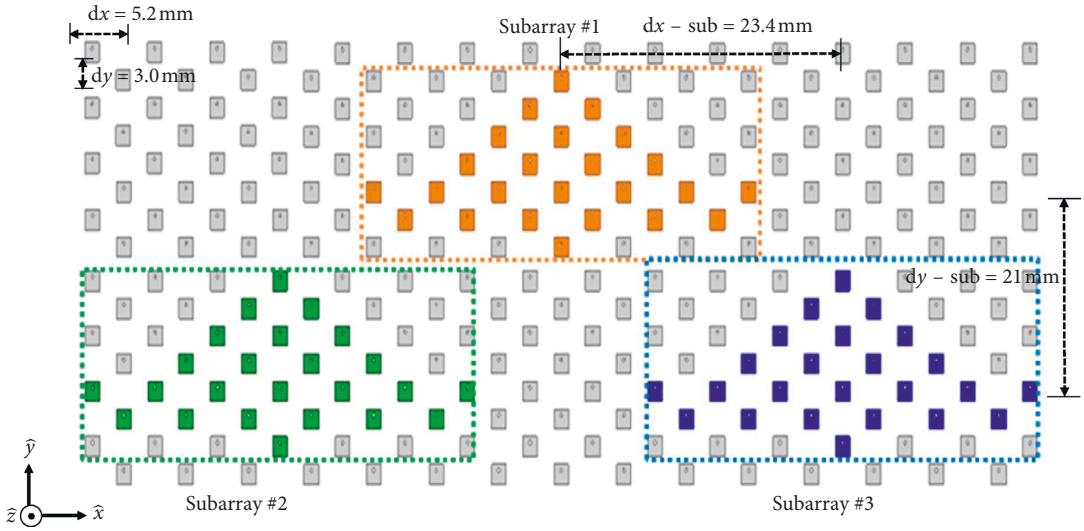

Figure 1: Configuration of the proposed array formed of three 24-element triangular-grid diamond-shaped subarrays. In the array, $dx = 5.2$ mm and $dy = 3.0$ mm.

No.22		No.16		No.10		No.7		No.1
	No.19		No.13		No.2		No.4	
No.23		No.17		No.11		No.8		No.2
	No.20		No.14		No.2		No.5	
No.24		No.18		No.12		No.9		No.3
	No.21		No.15		No.2		No.6	

Figure 2: Rectangular aperture.

						No.17 −7 dB						
					No.18 −3 dB		No.13 −3 dB					
				No.19 −3 dB		No.14 0 dB		No.9 −3 dB				
			No.20 −3 dB		No.15 0 dB		No.10 0 dB		No.5 −3 dB			
No.24 −19 dB		No.22 −6 dB		No.16 −1 dB		No.11 0 dB		No.6 −1 dB		No.3 −6 dB		No.1 −19 dB
	No.23 −12 dB		No.21 −8 dB		No.12 −2 dB		No.7 −2 dB		No.4 −8 dB		No.2 −12 dB	
						No.8 −6 dB						

Figure 3: Diamond-shaped aperture with adaptive nulling tapering in Mode II.

Table 1: Comparison of diamond-shaped and rectangular apertures.

Aperture	Element radiation power	Gain (dBi)	3-dB beamwidth in *xz*-plane (degree)	Sidelobe suppression (dB)	Mode
Rectangular	Uniform	19.4	9.6	13.0	—
Diamond shape	Uniform	19.4	7.6	17.9	Mode I
Diamond shape	Adaptive nulling tapering	15.5	9	35.8	Mode II

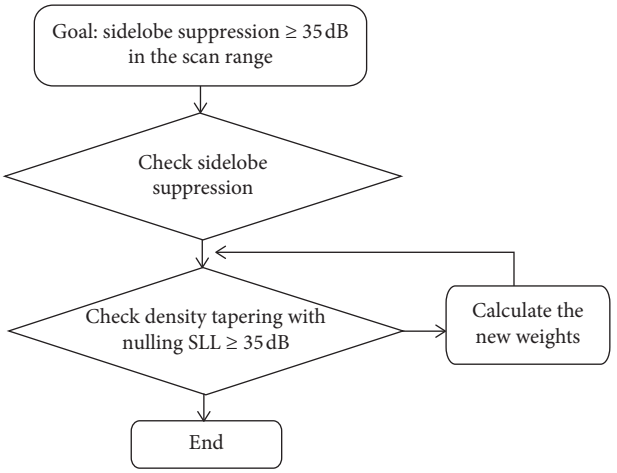

Figure 4: Iterative procedure of sidelobe suppression.

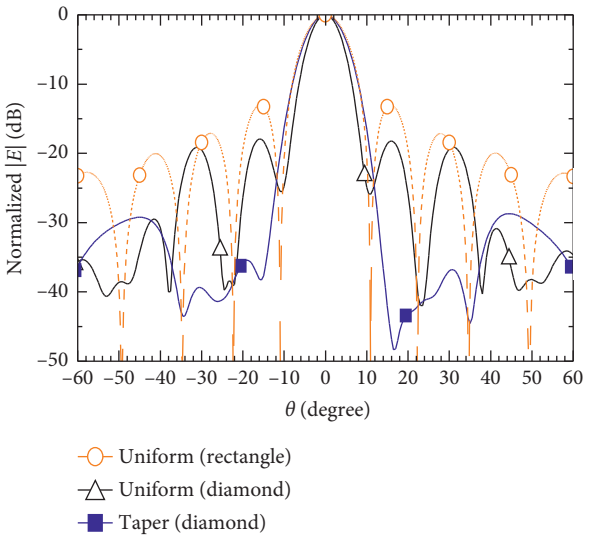

Figure 5: Simulated *xz*-plane normalized patterns of the subarray at 38 GHz for the rectangular aperture in Figure 2, the diamond-shaped aperture with uniform radiation power, and the diamond-shaped aperture with tapered radiation power.

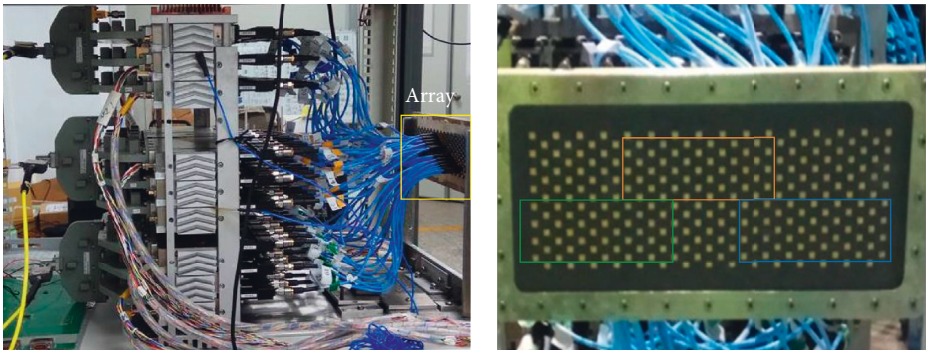

(a) (b)

Figure 6: Continued.

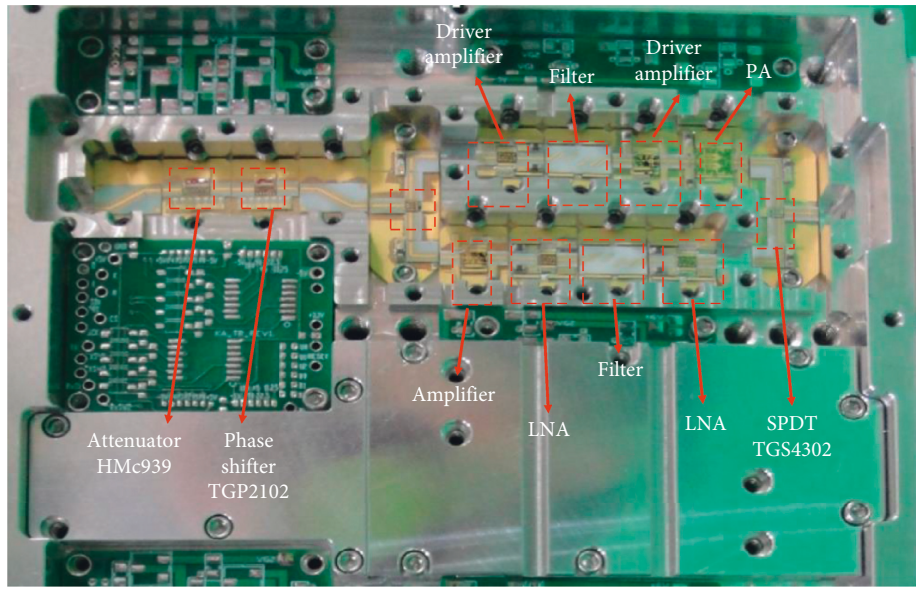

(c)

Figure 6: Photographs of feeding networks and the fabricated array: (a) side view, (b) three subarrays, and (c) Ka-band TRM.

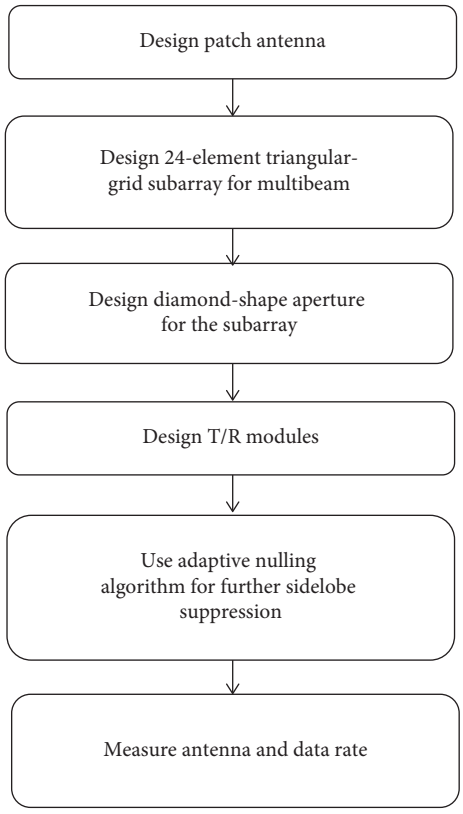

Figure 7: Overall design procedure.

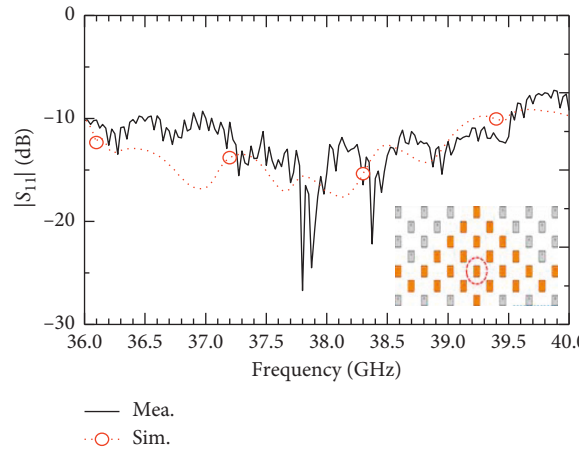

Figure 8: Simulated and measured reflection coefficients of the single patch. The patch is circled in the figure.

the measurements, the subarray is investigated in two different modes: Mode I and Mode II. In Mode I, all subarray elements are uniformly excited. In Mode II, the distribution of the element power attenuation, as shown in Figure 3, is set to achieve sidelobe suppression of more than 35 dB at $\theta = 20^\circ$.

Figure 9 shows the normalized simulated and measured radiation patterns of the subarray in Mode I. It can be seen that the sidelobe suppression is about 17.92 dB due to the effect of the x-direction density tapering in the diamond-shaped aperture. Figure 10 shows the normalized simulated and measured radiation patterns of the subarray in Mode II. For the subarray in Mode II, the sidelobe suppression is better than 35 dB from $\theta = 16^\circ$ to $\theta = 36^\circ$. As shown in Figure 11, the measured peak gain of the Mode I subarray is 19~19.6 dBi in the frequency range from 37 to 39 GHz. The measured peak gain of the Mode II subarray is reduced to 15~15.8 dBi in the frequency range from 37 to 39 GHz due to the sidelobe suppression. Figure 12 shows the measured xz-plane patterns of the subarray in Mode II at 38 GHz. With

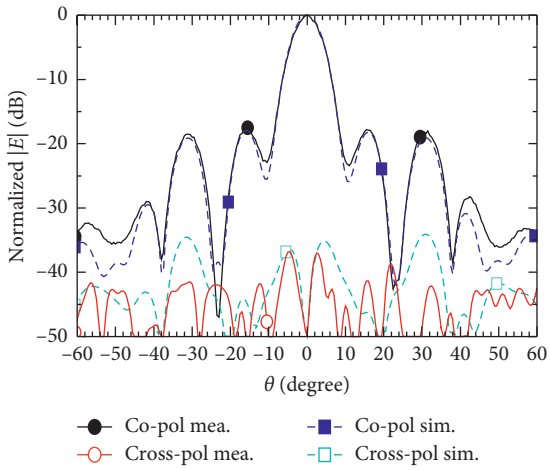

Figure 9: Measured and simulated *xz*-plane normalized patterns of the subarray in Mode I at 38 GHz.

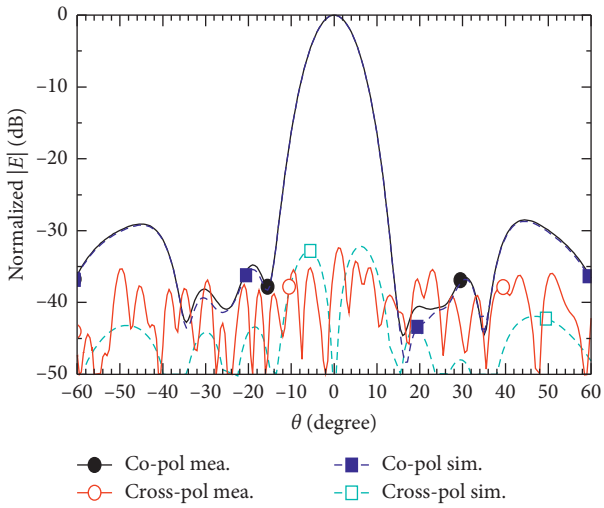

Figure 10: Measured and simulated *xz*-plane normalized patterns of the subarray in Mode II at 38 GHz.

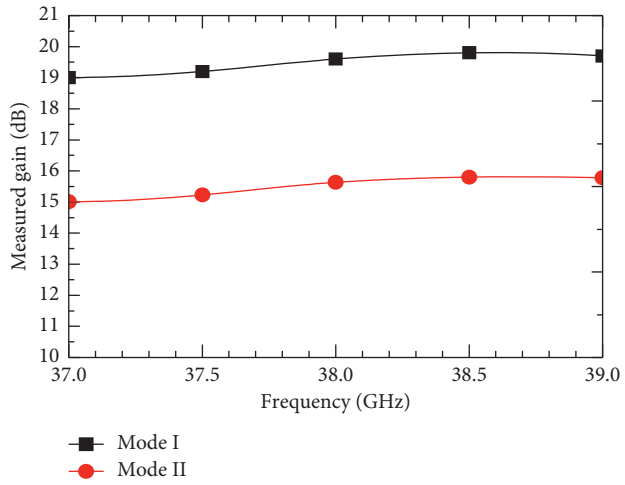

Figure 11: Measured peak gains of the subarray, with the main beam being in $\theta = 0^\circ$.

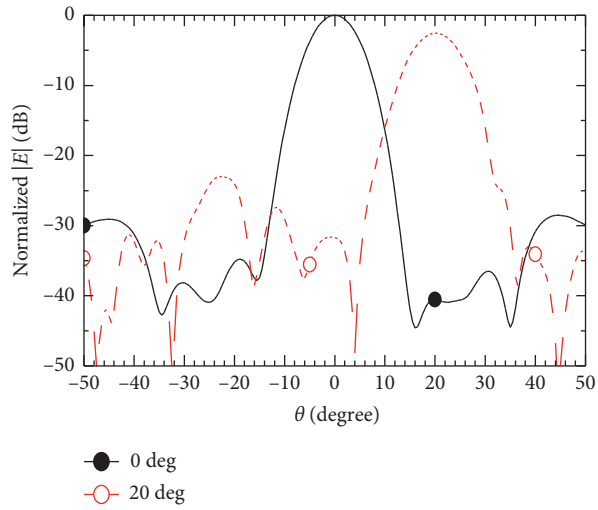

Figure 12: Measured *xz*-plane normalized patterns of the subarray in Mode II at 38 GHz, with the main beam being in $\theta = 0^\circ$ and $\theta = 20^\circ$.

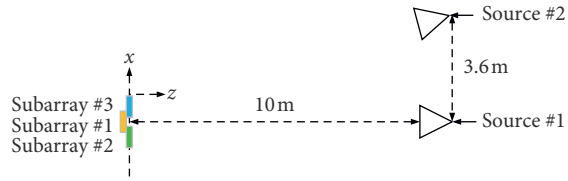

Figure 13: Experiment setup for the data-rate measurements.

the main beam pointed at $\theta = 0^\circ$, the 3 dB beamwidth is 9°, and the first sidelobe rejection at the left side is approximately −36 dB. When the main beam is pointed at 20°, the 3 dB beamwidth becomes 10° with the scan loss of about 2.5 dB.

The data-rate measurement is also conducted at 38 GHz by using the National Instruments millimetre-wave transceiver system [18]. As shown in Figure 13, the measurement setup consists of two testing dish antennas (Sources #1 and #2) and three patch subarrays (Subarray #1, Subarray #2, and Subarray #3). The target distance is chosen to be 10 m along the *z*-axis. The separation between two transmitted dish antennas is 3.6 m, so Source #1 transmits signal from $\theta = 0^\circ$ and Source #2 from $\theta = 20^\circ$. The millimetre-wave transceiver system is a 64 QAM modular reconfigurable prototyping platform for two-way communications. The software panel showing waveform, spectrum, constellation, SNR, and the measured data-rate performances are shown in Figure 14. Two measurements are conducted in the investigation. In the first measurement, the main beams of all subarrays are all pointed at $\theta = 0^\circ$, and only Source #1 transmits from $\theta = 0^\circ$. In this case, it is found that the data rates are better than 7 Gbps for both Mode I and Mode II, since there is no interference in the measurements. In the second measurement, in order to demonstrate the effect of sidelobe suppression, Sources #1 and #2 simultaneously transmit from $\theta = 0^\circ$ to $\theta = 20^\circ$, respectively, and all subarrays are still pointed at $\theta = 0^\circ$. It is found that, when the subarray is operated in Mode II, the

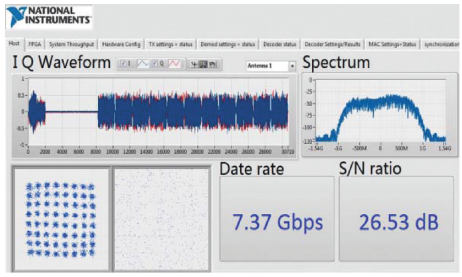

Figure 14: Software panel of the data-rate measurement system [14].

Table 2: Data rate and SNR measurement results.

Operation mode	Data rate (Gbps)	SNR (dB)
Mode I ($\theta = 0^\circ$)	7.37	26.53
Mode II ($\theta = 0^\circ$)	7.37	26.05
Mode I ($\theta = 0^\circ$ and $\theta = 20^\circ$)	4.62	17.82
Mode II ($\theta = 0^\circ$ and $\theta = 20^\circ$)	7.03	21.01

measured data rate is still better than 7 Gbps. For the subarray operated in Mode I with insufficient sidelobe suppression, the data rates are down to 4.62 Gbps. All the measured data in the data-rate investigation are given in Table 2.

4. Conclusion

A design of 38 GHz planar phased array with sidelobe suppression for data-rate enhancement is presented. The proposed array is formed of three 24-element subarrays of patches. The sidelobe suppression of the subarray is first improved to 17.92 dB with a diamond-shaped aperture and then better than 35 dB with a tapered radiation power distribution. The proposed design is validated with measurements. The effect of sidelobe suppression on the data rate is also demonstrated.

Data Availability

The experimental data used to support the findings of this study are included within the article.

Conflicts of Interest

The authors declare that there are no conflicts of interest regarding the publication of this paper.

Acknowledgments

This work was supported by the Ministry of Science and Technology, ROC, under grant MOST 108-2221-E-008-014-, and by National Chung-Shan Institute of Science and Technology, ROC.

References

[1] FCC, *Use of Spectrum Bands above 24 GHz for Mobile Radio*, FCC, Washington, DC, USA, 2015.

[2] N. Ojaroudiparchin, M. Shen, S. Zhang, and G. F. Pedersen, "A switchable 3-D-coverage-phased array antenna package for 5G mobile terminals," *IEEE Antennas and Wireless Propagation Letters*, vol. 15, no. 11, pp. 1747–1750, 2016.

[3] X. Gao, L. Dai, and A. M. Sayeed, "Low RF-Complexity technologies to enable millimeter-wave MIMO with large antenna array for 5G wireless communications," *IEEE Communications Magazine*, vol. 56, no. 4, pp. 211–217, 2018.

[4] H. L. Van Trees, *Optimum Array Processing: Part IV of Detection, Estimation, and Modulation Theory*, Wiley, NewYork, NY, USA, 2002.

[5] R. L. Haupt, *Antenna Arrays: A Computational Approach*, Wiley, Hoboken, NJ, USA, 2010.

[6] M. A. Sarker, M. S. Hossain, and M. S. Masud, "Robust beamforming synthesis technique for low side lobe level using taylor excited antenna array," in *Proceedings of the 2016 2nd International Conference on Electrical, Computer & Telecommunication Engineering*, pp. 1–4, Rajshahi, Bangladesh, December 2016.

[7] O. M. Bucci, M. D'Urso, T. Isernia, P. Angeletti, and G. Toso, "Deterministic synthesis of uniform amplitude sparse arrays via new density taper techniques," *IEEE Transactions on Antennas and Propagation*, vol. 58, no. 6, pp. 1949–1958, 2010.

[8] A. F. Morabito, A. Di Carlo, L. Di Donato, T. Isernia, and G. Sorbello, "Extending spectral factorization to array pattern synthesis including sparseness, mutual coupling, and mounting-platform effects," *IEEE Transactions on Antennas and Propagation*, vol. 67, no. 7, pp. 4548–4559, 2019.

[9] P. Rocca, R. L. Haupt, and A. Massa, "Interference suppression in uniform linear arrays through a dynamic thinning strategy," *IEEE Transactions on Antennas and Propagation*, vol. 59, no. 12, pp. 4525–4533, 2011.

[10] I. P. Gravas, Z. D. Zaharis, T. V. Yioultsis, P. I. Lazaridis, and T. D. Xenos, "Adaptive beamforming with sidelobe suppression by placing extra radiation pattern nulls," *IEEE Transactions on Antennas and Propagation*, vol. 67, no. 6, pp. 3853–3862, 2019.

[11] G. Buttazzoni and R. Vescovo, "Density tapering of linear arrays radiating pencil beams: a new extremely fast Gaussian approach," *IEEE Transactions on Antennas and Propagation*, vol. 65, no. 12, pp. 7372–7377, 2017.

[12] R. Chopra and G. Kumar, "Series-fed binomial microstrip arrays for extremely low sidelobe level," *IEEE Transactions on Antennas and Propagation*, vol. 67, no. 6, pp. 4275–4279, 2019.

[13] TGS4302 Datasheet, https://www.qorvo.com/products/p/TGS4302.

[14] TGP2102 Datasheet, https://www.qorvo.com/products/p/TGP2102.

[15] HMC939 Datasheet, https://www.analog.com/media/en/technical-documentation/data-sheets/hmc939chips.pdf.

[16] Ansoft Corporation, *Ansoft HFSS Ver. 14*, Ansoft Corporation, Canonsburg, PA, USA, 2010.

[17] NSI-MI Vertical Planar Near-Field System, http://www.nsi-mi.co.jp/literature/NSI-400V-23x22.

[18] National Instruments Millimeter-Wave Transceiver System, http://www.ni.com/sdr/mmwave/.